Theor Chem Acc (2010) 127:157–173
DOI 10.1007/s00214-009-0711-0

REGULAR ARTICLE

Spectroscopy of H_3^+ with energies above the barrier to linearity: rovibrational transitions in the range of 10,000–14,000 cm^{-1}

Ralph Jaquet

Received: 24 September 2009 / Accepted: 26 November 2009 / Published online: 19 December 2009

Abstract Based on a recently extended potential energy surface for H_3^+ with a highly reliable form of the topology of the surface far beyond the barrier to linearity, rovibrational frequencies in the range of 10,000–14,000 cm^{-1} have been derived and are compared with new experiments. The computed transition frequencies reproduce experimental transitions mostly within a few tenths of a wavenumber, if non-adiabatic effects are crudely simulated using different reduced masses for vibrational and rotational motions. Deviations can only be compensated if non-adiabatic effects are treated more rigorously.

Keywords Rovibrational energies · Non-adiabatic effects · Beyond barrier to linearity

1 Introduction

The theoretical investigations of spectra of polyatomic molecules based on first principles are nowadays a formidable task at least for triatomic systems with two or three hydrogen atoms, if one aims at highest, i.e. spectroscopic, accuracy. The deviations between calculated and experimental spectra depend on three different subjects: (a) the solution of the electronic Schrödinger equation, (b) the solution of the nuclear motion problem, and (c) the question whether the Born–Oppenheimer Ansatz is appropriate. Converged results can be reached for few electron systems with few degrees of freedom. The quality of the potential energy surface decides about the absolute accuracy of the rovibrational frequencies: (a) for scattering problems an extended region of the potential energy surface is needed, and consequently the ab initio calculations are mostly of inferior accuracy and (b) in case of spectroscopy a smaller local region of the potential energy surface is probed.

With two electrons and three protons, H_3^+ is the simplest polyatomic molecule; its equilibrium geometry is an equilateral triangle. H_3^+ is a rich source of information about ion chemistry, planetary atmospheres, unusual spectroscopic effects, etc., [1] and a benchmark molecule for theorists [2]. Most of the investigations have been performed for the electronic ground state which is a singlet state, although the triplet state is not of less interest at least for theoreticians [3]. Since H_3^+ is a fairly floppy molecule, it undergoes large-amplitude vibrational motions to such extent that the rovibrational spectrum does not confirm to many of the standard rules of spectroscopy.

In a very recent paper [4], we presented a new potential energy surface fit (termed BCJK) that is based on additional new 5,900 geometries (compared to the CRJK potential defined in Ref. [5]) with emphasis on non-equilibrium and asymptotic points. Apart from the Born–Oppenheimer energy converged to the accuracy better than 0.02 cm^{-1}, the adiabatic and the leading relativistic corrections are computed at each geometry. Possible choices of nuclear masses simulating the non-adiabatic effects in solving the nuclear Schrödinger equation had been analyzed. A small set of theoretically predicted rovibrational transitions were confronted with experimental data [6, 7] in the 10,700–13,700 cm^{-1} window of the spectrum.

What influences the accuracy of the rovibrational spectrum? The ab initio energy points of the clamped

Dedicated to the memory of Professor Jürgen Hinze and published as part of the Hinze Memorial Issue.

R. Jaquet (✉)
Theoretische Chemie, Universität Siegen,
57068 Siegen, Germany
e-mail: theo@theo.chemie.uni-siegen.de

nuclei electronic structure calculations are accurate up to $\Delta E \approx 0.02$ cm^{-1}, the accuracy of the adiabatic corrections is $\Delta E \approx 0.01$ cm^{-1}, and errors in the relativistic contributions are of the order $\Delta E \approx 0.01$ cm^{-1}. The values of the different contributions (BCJK fit [4]) vary with internuclear distances (relative to the value at the equilibrium distances and for $R(H_2\text{–}H) < 6$ bohr): 0–58,000 cm^{-1} (electronic energy), -22 to 55 cm^{-1} (diagonal adiabatic correction, the value at the equilibrium geometry is ≈ 115 cm^{-1}), and -2 to 1 cm^{-1} (relativistic contribution). The largest error originates from the fit of all contributions to the potential energy surface and depends on the polynomial fit; for the region around the minimum the error was mostly not smaller than $\Delta E \approx 0.05$ cm^{-1}, i.e., for polynomials we have used in recent works [4, 8–11]. Explicit non-adiabatic corrections are still missing, and are simulated by different masses for different nuclear motions, i.e., vibration and rotation. Additionally, the coupling to the electronically bound triplet state is assumed to be small and has not been taken into account. The effects of Lamb-shift have also been neglected.

The main motivation and goal of the recent work [4] was to extend the most accurate CRJK potential [5] to the regions which enable effective rovibrational analysis for transitions to states lying above the barrier to linearity. Beyond the barrier of linearity, which is $\approx 10{,}000$ cm^{-1} above the zero point energy, the density of energy states increases considerably. This leads to a stronger mixing (small energy denominators) of rovibrational energy levels with the same "good" quantum numbers. In addition, the treatment of nuclear motion in linear configurations can lead to singular behaviour (depending on the internal coordinates used) in the kinetic energy hamiltonian, which is inversely proportional to the moment of inertia, i.e., results achieved with different coordinate systems can deviate.

We have applied the same methodology, sketched shortly in the following section, as in Ref. [5] maintaining the convergence of the BO energy and computing the adiabatic and relativistic corrections for points located in the non-equilibrium and asymptotic regions of the PES.

In the meantime, data of new experiments [13, 14] are available, in which (a) using the dual-beam double-modulation technique (Morong et al. [13]), 143 transitions in the range of 10,300–13,700 cm^{-1} are observed, and (b) applying the method of action spectroscopy (Kreckel et al. [14]), developed by Schlemmer and Gerlich [15], 23 transitions in the range of 11,228–13,333 cm^{-1} have been found.

Whereas, we can compare our transition frequency calculations with both experimental transitions; IR intensities are given only in the first case. We will analyze the present status of agreement and disagreement between theory and experiments, and especially discuss how the inclusion of non-adiabatic effects will modify the results.

2 Methods

2.1 Contributions from the solution of the electronic Schrödinger equation

The potential energy E for the movement of the nuclei is composed of three contributions: the Born–Oppenheimer (clamped nuclei) energy E_{BO}, the adiabatic correction E_{ad}, and the relativistic correction E_{rel}

$$E = E_{BO} + E_{ad} + E_{rel}. \tag{1}$$

The BO energy E_{BO} was obtained by variationally solving the Schrödinger equation with the non-relativistic clamped nuclei Hamiltonian. The adiabatic correction E_{ad} and the relativistic correction E_{rel}, as significantly smaller than E_{BO}, were computed as the leading-order perturbative corrections to E_{BO}. The Ansatz for the electronic wave function uses two-electron basis functions known as Gaussian geminals (GG) [12].

The adiabatic correction was computed by means of the Born–Handy method [16] in which E_{ad} is evaluated as an expectation value of the nuclear kinetic energy operator expressed in laboratory coordinates

$$E_{ad} = \int \Psi(\boldsymbol{r}_1, \boldsymbol{r}_2) \left(-\sum_{I=1}^{3} \frac{\nabla_I^2}{2M_I} \right) \Psi(\boldsymbol{r}_1, \boldsymbol{r}_2)\, \mathrm{d}\boldsymbol{r}_1 \mathrm{d}\boldsymbol{r}_2. \tag{2}$$

In the above equation, M_I are the nuclear masses and Ψ is the electronic wave function dependent parametrically on the nuclear coordinates. This approach [17] can be considered superior to the classic approach based on the separation of the center of mass motion [18], because it is simpler (cartesian derivatives, and not molecule dependent coordinate derivatives) and includes all contributions (from relative vibrational, rotational and center of nuclear mass motion).

The leading relativistic correction had been calculated in the frames of the Direct Perturbation Theory (DPT) [19–23]. The lowest order correction can be obtained from the following expression [19, 24, 25]

$$E_{rel} = \langle \hat{H}_{BP} \rangle + \Delta_{DPT}, \quad \Delta_{DPT} = \frac{1}{2} c^{-2} \langle \hat{T} \left(\hat{H} - E_{BO} \right) \rangle \tag{3}$$

and $\langle \hat{H}_{BP} \rangle$ is the expectation value of the Breit-Pauli (BP) Hamiltonian computed with the non-relativistic wave function ($\hat{T}$ is the kinetic energy operator and $\hat{H}$ is the non-relativistic Hamiltonian).

The analytical fit to the computed energy points can be performed in different ways getting a global or local description. We choose a form where the electronic

energies, relativistic, and adiabatic contributions were added up for each point and a power series expansion in Morse-type symmetry adapted deformation coordinates was performed for the 16th order polynomial fit of the potential V. The weighted root mean square deviation (RMS) for the fit is 1.16 cm^{-1} and is based on 2,723 points limited to distances shorter than $R(H_2 - H) = 6a_0$. An increase in the range of the points to the dissociation limit leads to a poorer fit. Compared to former fits with an RMS of $\approx$0.05 cm^{-1} based only on 69 points, the new fit seems to be a change to the worse. If we would have used the original fit based on 69 points, the new energy points would be fitted in the following way: all points up to 20,000 cm^{-1} would have an RMS value of 3.69 cm^{-1} and all points surrounding the given 69 points (using Jacobi coordinates: with shifts of $\pm$0.003 bohr for r, $\pm$0.25 bohr for R, and $\pm 3°$ for the angle θ, as described in Ref. [4]) have an RMS value of 0.60 cm^{-1} and all new points together used in the present fit would have an RMS of 154.03 cm^{-1}. The present fit shows the following details: all points up to 20,000 cm^{-1} would have an RMS of 1.17 cm^{-1}, but a slightly worse RMS for all points surrounding the given 69 points of 0.86 cm^{-1}. Whereas the electronic potential is smoothly changing for increasing $R(H_2 - H)$, the adiabatic corrections show a steady increase at $r(H_2)$ for larger $R(H_2 - H)$ values, i.e. for $R > 6$ bohr. All the discussed details are a good reason not to rely on older fits based only on 69 points as mostly used in the past. More detailed information about the energy points is given in Ref. [4].

2.2 Solution of the nuclear Schrödinger equation

Perturbation theory is not reliable for the precise solution of vibrational and rotational problems of floppy molecules like H_3^+. In such difficult cases, variational methods have to be used, although, compared to perturbational calculations, their use is usually computationally more expensive [26].

In this paper, we report results of quantum mechanical variational calculations performed for the rovibrational states of H_3^+, using (a) the method of Sutcliffe and Tennyson for triatomic molecules (Jacobi coordinates), implemented in the program package DVR3DRJ [27], (b) using hyperspherical coordinates in conjunction with hyperspherical harmonics [28, 29], and (c) using a filter-diagonalization method [30] with a Fourier-DVR (discrete variable representation) grid for Jacobi coordinates [31–33]. We will not discuss the contributions coming from the different methods, but present results based on the adiabatic approximation and improvements related to non-adiabatic contributions. Details in respect to program suites, basis sets, etc. are given in Ref. [4].

The selection rules for the transitions can be summarized in the following way: the two possible vibrations are the totally symmetric mode v_1 and the double degenerate mode v_2. The degenerate mode v_2 gives rise to an vibrational angular momentum l. The vibrational angular momentum is strongly coupled to the overall rotation of the molecule, and thus k (the projection of the total rotation vector J) nor l are good quantum numbers. It became useful to define $G = |k - l|$ as a more 'robust' quantum number. For H_3^+ with three spin 1/2 nuclei one state with total spin $I = 3/2$ (ortho H_3^+) and two states with spin $I = 1/2$ (para H_3^+) are possible; the ortho/para statistical weights are 4/2. The nuclear spin wave function of ortho H_3^+ is totally symmetric with respect to exchange of the particles, while that of para H_3^+ is degenerate, i.e., partially antisymmetric. If one ignores the very small hyperfine interaction, three quantum numbers can be regarded as good: the total angular momentum J, the parity $\pm$ and the total nuclear spin angular momentum I. Rigorous selection rules are $\Delta J = 0$ or $\pm$ 1; $+, \leftrightarrow, -$, and $\Delta I = 0$ for single photon electric dipole transitions. The last selection rule can be interpreted in the sense that ortho ($G = 3n$) to para ($G = 3n \pm 1$) transitions are forbidden (n is integer). The parity change is related to $\Delta k = \pm 1$ (with parity = $(-1)^k$). Due to the symmetry restrictions some eigenstates do not exist—most notably the vibrationless states for J even and $G = 0$. The physical ground state of para H_3^+ is ($J = 1$, $K = 1$) (with $K = |k|$), but for ortho H_3^+ it is ($J = 1$, $K = 0$) [34]. Because the molecular symmetry group for H_3^+ is D_{3h}, transitions only between $A_2^{'} \leftrightarrow A_2^{''}$ (ortho) and $E' \leftrightarrow E''$ (para) states are allowed. For further details about symmetry, selection rules, assignments, and forbidden rotational transitions, see Lindsay and McCall [35].

The nuclear dynamics calculations can be performed with different choices of mass (e.g., nuclear or atomic masses). Depending on the level of theory (see [5] and [9]) used to generate the electronic potential, i.e., BO approximation, BO plus adiabatic contributions, etc., different masses are used within the nuclear Schrödinger equation. The reason for this technique is to simulate the experiment or to remove the deviations to complete theory [8, 36–38]. In the current study, we have used the nuclear mass **NU** = 1.0072764 amu. The influence of non-adiabatic effects can be simulated by considering the vibrational and rotational motion with different effective masses (**VR**) [10]. For the case of diatomic molecules, the idea of two different masses has been introduced by Bunker and Moss [36, 37] and rigorous formulas for the internuclear distance dependence of the masses have been derived in Refs. [39, 40, 42]. The analysis of H_2 has shown that adiabatic and non-adiabatic contributions to the frequencies are of the same order of magnitude. This means that if one aims at obtaining high accuracy data for spectroscopic properties or reaction dynamics, the concept of a typical, i.e., $E_{BO} + E_{ad}$, potential energy surface can no longer be justified; in our

Table 1 Comparison between experimental (Morong et al. [13]) and theoretical transitions (in cm^{-1}) with final and initial assignment of the rovibrational eigenstates using the masses VR

Vibration	Rotation	EXP	VR	Δ(EXP-VR)	Int. (EXP)	Int. (calc)	E′(VR)	E″(VR)
$2v_1 + 2v_2^2 \leftarrow 0$	^{t}P(3, 0)	10,322.235	10,321.661	0.574	14.0	10.605	516.909	10,838.570
unknown $\leftarrow 0$	R(6, 6)	10,329.307	10,328.852	0.455	22.7	19.777	995.648	11,324.500
$0v_1 + 4v_2^4 \leftarrow 0$	^{n}R(2, 2)	10,366.546	10,366.025	0.521	16.8	20.873	169.279	10,535.304
$0v_1 + 4v_2^4 \leftarrow 0$	^{n}R(2, 1)	10,367.184	10,366.625	0.559	43.2	10.937	237.363	10,603.988
$0v_1 + 4v_2^4 \leftarrow 0$	^{n}R(3, 3)	10,454.539	10,453.990	0.549	44.3	63.511	315.297	10,769.287
unknown $\leftarrow 0$	P(6, 6)	10,462.405	10,461.847	0.558	31.7	26.683	995.648	11,457.495
$2v_1 + 2v_2^2 \leftarrow 0$	^{t}Q(2, 1)	10,467.800	10,467.204	0.596	8.2	7.343	237.363	10,704.567
$2v_1 + 2v_2^2 \leftarrow 0$	^{t}Q(3, 1)	10,468.544	10,467.951	0.593	11.5	7.680	494.782	10,962.733
unknown $\leftarrow 0$	R(5, 5)	10,496.287	10,495.718	0.569	14.6	14.505	728.858	11,224.576
$2v_1 + 2v_2^2 \leftarrow 0$	^{n}P(2, 1)	10,496.571	10,496.036	0.535	6.3	7.201	237.363	10,733.399
$2v_1 + 2v_2^2 \leftarrow 0$	^{t}R(4, 4)	10,497.078	10,496.495	0.583	40.7	34.325	501.939	10,998.434
$2v_1 + 2v_2^2 \leftarrow 0$	^{n}P(3, 2)	10,507.396	10,506.867	0.529	6.6	9.562	428.012	10,934.879
$2v_1 + 2v_2^2 \leftarrow 0$	^{n}P(4, 3)	10,528.992	10,528.479	0.513	6.3	8.151	658.681	11,187.160
$2v_1 + 2v_2^2 \leftarrow 0$	^{n}P(5, 5)^l	10,558.882	10,558.440	0.442	42.9	26.020	728.858	11,287.298
$2v_1 + 2v_2^2 \leftarrow 0$	^{t}Q(3, 0)	10,560.443	10,559.872	0.571	31.8	27.711	516.909	11,076.781
$2v_1 + 2v_2^2 \leftarrow 0$	^{t}Q(1, 0)	10,568.209	10,567.644	0.565	30.1	40.690	86.966	10,654.610
unknown $\leftarrow 0$	R(4, 3)	10,573.997	10,573.465	0.532	23.9	21.369	658.681	11,232.146
$2v_1 + 2v_2^2 \leftarrow 0$	^{n}P(1, 1)	10,581.256	10,580.719	0.537	9.8	6.994	64.120	10,644.839
$2v_1 + 2v_2^2 \leftarrow 0$	^{n}P(3, 3)	10,583.688	10,583.179	0.509	27.0	31.577	315.297	10,898.476
$2v_1 + 2v_2^2 \leftarrow 0$	^{n}P(2, 2)	10,586.424	10,585.908	0.516	8.9	14.919	169.279	10,755.187
$2v_1 + 2v_2^2 \leftarrow 0$	^{t}R(3, 3)	10,609.077	10,608.468	0.609	27.6	32.054	315.297	10,923.765
$2v_1 + 2v_2^2 \leftarrow 0$	^{t}R(2, 2)	10,621.634	10,621.032	0.602	35.8	27.573	169.279	10,790.311
$0v_1 + 5v_2^1 \leftarrow 0$	P(4, 3)	10,624.888	10,624.139	0.749	42.9	38.315	658.681	11,282.820
$0v_1 + 5v_2^1 \leftarrow 0$	P(4, 4)	10,632.042	10,631.406	0.636	47.3	37.567	501.939	11,133.345
unknown $\leftarrow 0$	Q(5, 0)	10,639.058	10,638.167	0.891	15.3	9.367	1,271.326	11,909.493
$2v_1 + 2v_2^2 \leftarrow 0$	^{t}R(1, 1)	10,641.024	10,640.447	0.577	27.6	24.110	64.120	10,704.567
$0v_1 + 5v_2^3 \leftarrow 0$	$^{+6}$Q(3, 0)	10,657.149	10656.350	0.799	22.2	20.025	516.909	11,173.259
unknown $\leftarrow 0$	Q(5, 3)	10,666.604	10,665.876	0.728	20.2	9.087	1,080.470	11,746.346
$2v_1 + 2v_2^2 \leftarrow 0$	^{n}Q(1, 1)	10,669.815	10,669.279	0.536	15.0	12.326	64.120	10,733.399
$2v_1 + 2v_2^2 \leftarrow 0$	^{n}Q(2, 1)	10,671.864	10,671.323	0.541	8.8	10.838	237.363	10,908.686
$2v_1 + 2v_2^2 \leftarrow 0$	^{n}P(4, 4)^u	10,686.611	10,685.908	0.703	33.3	4.642	501.939	11,187.847
$2v_1 + 2v_2^2 \leftarrow 0$	^{t}R(4, 3)	10,690.240	10,689.652	0.588	25.2	20.257	658.681	11,348.333
$2v_1 + 2v_2^2 \leftarrow 0$	^{t}R(3, 2)	10,705.364	10,704.549	0.815	15.8	18.579	428.012	11,132.561
$0v_1 + 5v_2^1 \leftarrow 0$	P(3, 2)	10,705.894	10,705.086	0.808	9.3	16.958	428.012	11,133.098
$0v_1 + 5v_2^1 \leftarrow 0$	Q(4, 3)^u	10,710.311	10,709.222	1.089	48.6	13.000	658.681	11,367.903
$2v_1 + 2v_2^2 \leftarrow 0$	^{t}R(2, 1)	10,725.953	10,725.370	0.583	18.1	20.129	237.363	10,962.733
$0v_1 + 5v_2^1 \leftarrow 0$	P(3, 3)	10,730.107	10,729.360	0.747	64.9	100.000[b]	315.297	11,044.657
$2v_1 + 2v_2^2 \leftarrow 0$	^{t}R(1, 0)	10,752.150	10,751.604	0.546	58.8	58.953	86.966	10,838.570
$0v_1 + 5v_2^1 \leftarrow 0$	P(2, 2)	10,752.369	10,751.647	0.722	31.2	33.478	169.279	10,920.926
$2v_1 + 2v_2^2 \leftarrow 0$	^{n}Q(3, 2)^u	10,760.627	10,759.835	0.792	4.1	4.297	428.012	11,187.847
$0v_1 + 5v_2^1 \leftarrow 0$	P(2, 1)	10,766.320	10,765.528	0.792	13.0	16.444	237.363	11,002.891
$2v_1 + 2v_2^2 \leftarrow 0$	^{n}Q(2, 2)	10,766.108	10,765.600	0.508	10.9	10.572	169.279	10,934.879
$0v_1 + 5v_2^1 \leftarrow 0$	Q(3, 2)^u	10,779.136	10,778.605	0.531	13.6	24.853	428.012	11,206.617
$0v_1 + 5v_2^3 \leftarrow 0$	$^{+6}$Q(2, 1)	10,789.844	10,789.121	0.723	22.0	33.237	237.363	11,026.484
$2v_1 + 2v_2^2 \leftarrow 0$	^{n}Q(4, 2)^u	10,793.060	10,792.551	0.509	8.0	8.051	768.482	11,561.033
$0v_1 + 5v_2^1 \leftarrow 0$	P(3, 0)	10,798.691	10,797.837	0.854	21.2	20.933	516.909	11,314.746
$0v_1 + 5v_2^1 \leftarrow 0$	P(1, 1)	10,798.785	10,798.050	0.735	12.6	17.117	64.120	10,862.170

Table 1 continued

Vibration	Rotation	EXP	VR	Δ(EXP-VR)	Int. (EXP)	Int. (calc)	E′(VR)	E″(VR)
$0v_1 + 5v_2^3 \leftarrow 0$	$^{+6}$Q(3, 1)	10,803.820	10,802.955	0.865	26.6	28.419	494.782	11,297.737
$2v_1 + 2v_2^2 \leftarrow 0$	^{t}R(3, 1)	10,805.800	10,805.189	0.611	10.7	9.781	494.782	11,299.971
$0v_1 + 5v_2^1 \leftarrow 0$	P(5, 3)^{l}	10,811.027	10,810.240	0.787	15.8	10.986	1,080.470	11,890.710
$0v_1 + 5v_2^1 \leftarrow 0$	P(3, 1)	10,813.699	10,812.893	0.806	11.6	10.867	494.782	11,307.675
$0v_1 + 5v_2^3 \leftarrow 0$	$^{+6}$Q(4, 1)	10,816.758	10,815.952	0.806	15.5	12.827	833.620	11,649.572
$0v_1 + 5v_2^1 \leftarrow 0$	Q(1, 0)	10,831.677	10,830.937	0.740	100.0	87.399	86.966	10,917.903
$2v_1 + 2v_2^2 \leftarrow 0$	^{n}R(1, 1)	10,845.089	10,844.566	0.523	12.1	7.753	64.120	10,908.686
$2v_1 + 2v_2^2 \leftarrow 0$	^{n}Q(4, 3)	10,847.551	10,847.162	0.389	16.0	15.930	658.681	11,505.843
$0v_1 + 5v_2^1 \leftarrow 0$	Q(4, 2)^{u}	10,855.172	10,854.226	0.946	7.8	9.237	768.482	11,622.708
$3v_1 + 1v_2^1 \leftarrow 0$	P(6, 6)	10,874.681	10,874.482	0.199	25.5	15.470	995.648	11,870.130
$2v_1 + 2v_2^2 \leftarrow 0$	^{n}R(2, 1)	10,934.327	10,933.793	0.534	14.9	11.125	237.363	11,171.156
$0v_1 + 5v_2^1 \leftarrow 0$	Q(3, 0)	10,935.631	10,934.519	1.112	53.7	46.207	516.909	11,451.428
$2v_1 + 2v_2^2 \leftarrow 0$	^{t}R(3, 0)	10,935.358	10,935.083	0.275	44.9	43.276	516.909	11,451.992
$0v_1 + 5v_2^1 \leftarrow 0$	Q(1, 1)	10,939.559	10,938.771	0.788	23.3	23.386	64.120	11,002.891
$3v_1 + 1v_2^1 \leftarrow 0$	P(5, 5)	10,953.026	10,953.056	−0.030	6.5	10.559	728.858	11,681.914
$0v_1 + 5v_2^3 \leftarrow 0$	$^{+6}$R(1 ,1)	10,963.072	10,962.364	0.708	10.3	13.243	64.120	11,026.484
$0v_1 + 5v_2^1 \leftarrow 0$	Q(2, 2)	10,964.605	10,963.819	0.786	11.3	14.484	169.279	11,133.098
$0v_1 + 5v_2^1 \leftarrow 0$	$^{+6}$R(2, 2)	10,964.792	10,964.066	0.726	6.3	5.005	169.279	11,133.345
$0v_1 + 5v_2^1 \leftarrow 0$	Q(3, 3)	10,968.257	10,967.523	0.734	14.9	26.756	315.297	11,282.820
$3v_1 + 1v_2^1 \leftarrow 0$	P(4, 3)	11,015.488	11,015.051	0.437	13.8	10.038	658.681	11,673.732
$2v_1 + 2v_2^2 \leftarrow 0$	^{n}R(2, 2)^{u}	11,019.351	11,018.568	0.783	35.8	31.590	169.279	11,187.847
$2v_1 + 2v_2^2 \leftarrow 0$	^{n}R(3, 1)^{u}	11,024.705	11,024.852	−0.147	4.9	9.107	494.782	11,519.634
$3v_1 + 1v_2^1 \leftarrow 0$	P(4, 4)	11,033.268	11,032.858	0.410	16.1	11.580	501.939	11,534.797
unknown $\leftarrow 0$	R(6, 6)	11,036.111	11,035.493	0.618	23.1	2.887	995.648	12,031.141
$0v_1 + 5v_2^1 \leftarrow 0$	R(1, 1)^{l}	11,044.146	11,043.282	0.864	11.6	17.333	64.120	11,107.402
unknown $\leftarrow 0$	R(5, 5)	11,046.569	11,046.010	0.559	29.4	0.666	728.858	11,774.868
unknown $\leftarrow 0$	R(4, 4)	11,048.996	11,048.279	0.717	20.2	11.041	501.939	11,550.218
$0v_1 + 5v_2^1 \leftarrow 0$	R(3, 3)^{u}	11,053.686	11,052.606	1.080	90.2	50.768	315.297	11,367.903
$0v_1 + 5v_2^1 \leftarrow 0$	Q(2, 1)^{u}	11,071.117	11,070.312	0.805	7.3	8.056	237.363	11307.675
$3v_1 + 1v_2^1 \leftarrow 0$	P(3, 3)	11,111.798	11,111.362	0.436	19.9	21.273	315.297	11,426.659
$2v_1 + 2v_2^0 \leftarrow 0$	^{n}R(4, 3)	11,114.428	11,113.883	0.545	6.0	10.359	658.681	11,772.564
unknown $\leftarrow 0$	R(5, 0)	11,114.628	11,114.093	0.535	8.4	10.291	1,271.326	12,385.419
$0v_1 + 5v_2^1 \leftarrow 0$	R(3, 2)^{u}	11,195.625	11,194.696	0.929	9.7	7.632	428.012	11,622.708
$0v_1 + 5v_2^1 \leftarrow 0$	R(1, 0)	11,228.601	11,227.780	0.821	82.4	73.623	86.966	11,314.746
$0v_1 + 5v_2^1 \leftarrow 0$	R(1, 1)^{u}	11,244.353	11,243.555	0.798	15.2	17.937	64.120	11,307.675
$0v_1 + 5v_2^1 \leftarrow 0$	R(2, 1)^{l}	11,246.707	11,245.879	0.828	17.9	13.750	237.363	11,483.242
$3v_1 + 1v_2^1 \leftarrow 0$	Q(3, 0)	11,278.517	11,278.048	0.469	13.3	11.189	516.909	11,794.957
$0v_1 + 5v_2^1 \leftarrow 0$	R(2, 2)^{l}	11,304.480	11,303.658	0.822	18.8	16.757	169.279	11,472.937
$3v_1 + 1v_2^1 \leftarrow 0$	Q(1, 0)	11,318.080	11,317.612	0.468	15.5	13.087	86.966	11,404.578
unknown $\leftarrow 0$	P(6 ,6)	11331.112	11,330.560	0.552	14.9	10.854	995.648	12,326.208
$3v_1 + 1v_2^1 \leftarrow 0$	Q(3, 3)	11358.855	11,358.435	0.420	7.6	6.342	315.297	11,673.732
$0v_1 + 5v_2^1 \leftarrow 0$	$^{-6}$P(5, 5)^{u}	11,422.627	11,422.068	0.559	6.9	8.950	728.858	12,150.926
$0v_1 + 5v_2^3 \leftarrow 0$	$^{-6}$P(4, 4)	11,482.938	11,482.384	0.554	7.4	10.463	501.939	11,984.323
$0v_1 + 5v_2^5 \leftarrow 0$	P(4, 3)^{c}	11,496.055	11,495.581	0.474	12.0	13.262	658.681	12,154.262
$0v_1 + 5v_2^3 \leftarrow 0$	P(3, 3)^{c}	11,494.835	11,494.341	0.494	6.9	6.567	315.297	11,809.638
$0v_1 + 5v_2^1 \leftarrow 0$	R(2, 1)^{u}	11,496.796	11,496.011	0.785	16.7	16.842	237.363	11,733.374
$3v_1 + 1v_2^1 \leftarrow 0$	R(1, 0)	11,503.614	11,503.149	0.465	11.3	8.631	86.966	11,590.115

Table 1 continued

Vibration	Rotation	EXP	VR	Δ(EXP-VR)	Int. (EXP)	Int. (calc)	E′(VR)	E″(VR)
$0v_1 + 5v_2^3 \leftarrow 0$	$^{+6}$R(3, 2)	11,515.921	11,515.139	0.782	16.3	14.683	428.012	11,943.151
unknown $\leftarrow 0$	R(4, 3)	11,556.914	11,556.077	0.837	35.7	31.088	658.681	12,214.758
$1v_1 + 4v_2^0 \leftarrow 0$	^{t}Q(3, 0)	11562.798	11562.136	0.662	10.6	10.874	516.909	12,079.045
$0v_1 + 5v_2^5 \leftarrow 0$	$^{+6}$Q(3, 1)	11,564.098	11,563.451	0.647	7.7	6.581	494.782	12,058.233
$0v_1 + 5v_2^5 \leftarrow 0$	P(3, 3)	11,571.876	11,571.300	0.576	20.5	19.795	315.297	11,886.597
$0v_1 + 5v_2^1 \leftarrow 0$	R(3, 3)^{l}	11,576.154	11,575.413	0.741	31.0	32.847	315.297	11,890.710
$0v_1 + 5v_2^5 \leftarrow 0$	$^{+6}$P(2, 2)	11,578.494	11,577.926	0.568	18.7	9.688	169.279	11,747.205
$0v_1 + 5v_2^5 \leftarrow 0$	$^{+6}$Q(1, 0)	11,606.157	11,605.575	0.582	19.5	20.450	86.966	11,692.541
$0v_1 + 5v_2^1 \leftarrow 0$	R(3, 0)	11,618.521	11,617.830	0.691	8.4	8.086	516.909	12,134.739
$3v_1 + 1v_2^1 \leftarrow 0$	R(3, 3)^{u}	11,668.916	11,667.622	1.294	28.4	8.909	315.297	11,982.919
$0v_1 + 5v_2^3 \leftarrow 0$	Q(3, 0)	11,691.577	11,690.906	0.671	8.2	8.308	516.909	12,207.815
$0v_1 + 5v_2^5 \leftarrow 0$	$^{+6}$R(2, 2)	11,694.789	11,694.155	0.634	9.5	10.057	169.279	11,863.434
$0v_1 + 5v_2^5 \leftarrow 0$	$^{+6}$R(1, 1)	11,707.268	11,706.666	0.602	8.9	9.084	64.120	11,770.786
$0v_1 + 5v_2^5 \leftarrow 0$	$^{+6}$Q(1, 1)	11,707.801	11,707.199	0.602	6.1	6.488	64.120	11,771.319
$0v_1 + 5v_2^5 \leftarrow 0$	$^{+6}$R(3, 1)	11,728.382	11,727.658	0.724	12.8	6.974	494.782	12,222.440
$0v_1 + 5v_2^3 \leftarrow 0$	Q(2, 2)	11,788.272	11,787.682	0.590	5.1	5.833	169.279	11,956.961
$0v_1 + 5v_2^5 \leftarrow 0$	$^{+6}$R(3, 2)	11,793.656	11,792.977	0.679	6.4	7.255	428.012	12,220.989
$0v_1 + 5v_2^5 \leftarrow 0$	$^{+6}$R(3, 0)	11,835.025	11,834.273	0.752	15.7	15.771	516.909	12,351.182
$0v_1 + 5v_2^5 \leftarrow 0$	Q(3, 3)	11,839.565	11,838.965	0.600	10.0	10.167	315.297	12,154.262
$0v_1 + 5v_2^5 \leftarrow 0$	$^{+6}$R(1, 0)	11,854.459	11,853.850	0.609	26.0	23.973	86.966	11,940.816
$3v_1 + 1v_2^1 \leftarrow 0$	$^{-6}$R(4, 4)^{l}	11,892.128	11,893.581	−1.453	7.1	6.671	501.939	12,395.520
unknown $\leftarrow 0$	P(6, 6)	11,947.074	11,947.169	−0.095	5.0	5.499	995.648	12,942.817
$0v_1 + 5v_2^3 \leftarrow 0$	R(3, 3)	11,953.935	11,953.290	0.645	9.4	9.132	315.297	12,268.587
$1v_1 + 4v_2^0 \leftarrow 0$	^{t}R(3, 0)	11,978.640	11,977.944	0.696	8.6	9.680	516.909	12,494.853
$1v_1 + 4v_2^0 \leftarrow 0$	^{n}R(2, 2)	12,097.708	12,097.080	0.628	8.4	7.577	169.279	12,266.359
$1v_1 + 4v_2^2 \leftarrow 0$	^{t}R(3, 3)	12,102.469	12,100.971	1.498	2.0	5.806	315.297	12,416.268
unknown $\leftarrow 0$	Q(3, 0)	12116.353	12116.264	0.089	8.7	1.374	516.909	12,633.173
$1v_1 + 4v_2^4 \leftarrow 0$	^{t}P(4, 3)	12,181.941	12,181.313	0.628	4.3	8.031	658.681	12,839.994
$2v_1 + 3v_2^1 \leftarrow 0$	Q(2, 1)^{l}	12,207.905	12,207.584	0.321	6.9	5.782	237.363	12,444.947
$2v_1 + 3v_2^1 \leftarrow 0$	P(2, 2)	12,222.032	12,221.800	0.232	9.1	8.690	169.279	12,391.079
$1v_1 + 4v_2^2 \leftarrow 0$	^{t}R(1, 0)	12,246.368	12,245.642	0.726	7.1	7.398	86.966	12,332.608
$2v_1 + 3v_2^1 \leftarrow 0$	P(3, 3)	12,246.574	12,245.736	0.838	15.5	17.048	315.297	12,561.033
$2v_1 + 3v_2^1 \leftarrow 0$	Q(1, 0)	12,253.670	12,253.348	0.322	19.5	18.549	86.966	12,340.314
$1v_1 + 4v_2^2 \leftarrow 0$	^{n}Q(4, 3)	12,314.977	12,314.245	0.732	6.8	6.540	658.681	12,972.926
$0v_1 + 5v_2^5 \leftarrow 0$	R(3, 3)	12,320.975	12,320.368	0.607	6.7	7.018	315.297	12,635.665
unknown $\leftarrow 0$	R(4, 3)	12,331.180	12,330.386	0.794	7.8	5.011	658.681	12,989.067
$0v_1 + 6v_2^2 \leftarrow 0$	^{t}Q(1, 0)	12,419.140	12,418.969	0.171	14.2	7.491	86.966	12,505.935
unknown $\leftarrow 0$	P(3 ,3)	12,502.614	12,502.101	0.513	11.0	16.225	315.297	12,817.398
$1v_1 + 4v_2^4 \leftarrow 0$	^{t}Q(3, 3)	12,525.302	12,524.697	0.605	11.5	5.885	315.297	12,839.994
unknown $\leftarrow 0$	R(3, 0)	12,536.621	12,535.981	0.640	6.8	7.723	516.909	13,052.890
$1v_1 + 4v_2^4 \leftarrow 0$	^{t}Q(1, 1)	12,623.171	12,622.549	0.622	9.9	5.443	64.120	12,686.669
$1v_1 + 4v_2^2 \leftarrow 0$	^{n}R(3, 3)	12,658.335	12,657.629	0.706	24.1	17.631	315.297	12,972.926
$1v_1 + 4v_2^4 \leftarrow 0$	^{t}R(1, 0)	12,897.888	12,897.240	0.648	6.1	8.592	86.966	12,984.206
unknown $\leftarrow 0$	R(1, 0)	13,056.013	13,055.146	0.867	13.8	14.353	86.966	13,142.112
unknown $\leftarrow 0$	Q(1, 0)	13,597.367	13,596.740	0.627	5.1	7.849	86.966	13,683.706
unknown $\leftarrow 0$	R(3, 3)	13,606.093	13,605.147	0.946	6.5	6.442	315.297	13,920.444
unknown $\leftarrow 0$	Q(1, 0)	13,676.446	13,677.708	−1.262	6.4	1.739	86.966	13,764.674
unknown $\leftarrow v_2^1$	R(2, 0)	10,827.764	10,826.965	0.799	1.9	0.335	2812.639	13,639.604

Table 1 continued

Vibration	Rotation	EXP	VR	Δ(EXP-VR)	Int. (EXP)	Int. (calc)	E′(VR)	E″(VR)
unknown ← v_2^1	R(2, 0)	11,265.189	11,261.211	3.978	1.3	10^{-4}	3409.725	14,670.936

Intensities are calculated at 600 K and normalized to the highest line in the range from 10,000 to 14,000 cm^{-1}. The convention of assignment is established in Ref. [35]: vibrational band of the upper state ($v_1v_1 + v_2v_2^{l,l}$) and rotational transitions $\left({}^{[n|t|\pm6|\pm9|..]}\{P|Q|R\}(J,G)\frac{[u|l]}{[u|l]}\right)$. E(NU) result from **HYP** calculations. E(VR) = E(NU, HYP) + (E(VR, DVRJ) − E(NU, DVRJ)), i.e., the 'non-adiabatic' correction is calculated with the DVR-J code

[a] Different to Table 1 in Ref. [13]

[b] The Einstein A_{12} coefficient at 10,729.370 cm^{-1} is 2.18917 s^{-1} as described in Ref. [27]

Table 2 Comparison between experimental (Kreckel et al. [14]) and theoretical transitions (in cm^{-1}) with final and initial assignment of the rovibrational eigenstates using the masses VR

Vibration	Rotation	EXP	VR	Δ(EXP-VR)	Int. (calc)	E′(VR)	E″(VR)
$0v_1 + 5v_2^1 \leftarrow 0$	R(1, 0)	11,228.598	11,227.780	0.818	73.623	86.966	11,314.746
$0v_1 + 5v_2^1 \leftarrow 0$	R(1, 1)^u	11,244.350	11,243.555	0.795	17.937	64.120	11,307.675
$3v_1 + 1v_2^1 \leftarrow 0$	P(1, 1)	11,258.975	11,258.518	0.457	2.683	64.120	11,322.638
$3v_1 + 1v_2^1 \leftarrow 0$	Q(1, 1)	11,342.587	11,342.142	0.445	3.698	64.120	11,406.262
$3v_1 + 1v_2^1 \leftarrow 0$	R(1, 1)^l	11,465.505	11,465.046	0.459	3.367	64.120	11,529.166
$3v_1 + 1v_2^1 \leftarrow 0$	R(1, 1)^u	11,511.373	11,510.928	0.445	1.973	64.120	11,575.048
$0v_1 + 5v_2^5 \leftarrow 0$	$^{-6}$P(1, 1)	11,594.276	11,593.726	0.550	3.753	64.120	11,657.846
$0v_1 + 5v_2^5 \leftarrow 0$	$^{-6}$R(1, 1)	11,707.257	11,706.666	0.591	9.084	64.120	11,770.786
$0v_1 + 5v_2^5 \leftarrow 0$	$^{-6}$Q(1, 1)	11,707.797	11,707.199	0.598	6.488	64.120	11,771.319
$1v_1 + 4v_2^0 \leftarrow 0$	^{n}R(1, 1)	11,882.376	11,881.782	0.594	2.648	64.120	11,945.902
$1v_1 + 4v_2^2 \leftarrow 0$	^{t}Q(1, 0)	12,018.812	12,018.231	0.581	2.706	86.966	12,105.197
$1v_1 + 4v_2^2 \leftarrow 0$	^{t}R(1, 1)	12,086.738	12,086.121	0.617	4.431	64.120	12,150.241
$2v_1 + 3v_2^1 \leftarrow 0$	P(1, 1)	12,239.242	12,238.919	0.323	3.957	64.120	12,303.039
$2v_1 + 3v_2^1 \leftarrow 0$	Q(1, 1)	12,373.325	12,372.715	0.610	2.393	64.120	12,436.835
$2v_1 + 3v_2^1 \leftarrow 0$	R(1, 1)	12,381.135	12,380.827	0.308	2.322	64.120	12,444.947
$0v_1 + 6v_2^2 \leftarrow 0$	^{n}P(1, 1)	12,413.257	12,413.205	0.052	2.267	64.120	12,477.325
$0v_1 + 6v_2^2 \leftarrow 0$	^{t}Q(1, 0)	12,419.127	12,418.969	0.158	7.491	86.966	12,505.935
$0v_1 + 6v_2^2 \leftarrow 0$	^{n}Q(1, 1)	12,623.160	12,622.549	0.611	5.443	64.120	12,686.669
$0v_1 + 6v_2^2 \leftarrow 0$	^{t}R(1, 1)	12,678.683	12,677.978	0.705	5.446	64.120	12,742.098
$1v_1 + 4v_2^4 \leftarrow 0$	^{t}R(1, 0)	12,897.877	12,897.240	0.637	8.592	86.966	12,984.206
$0v_1 + 6v_2^2 \leftarrow 0$	^{t}R(1, 0)	13,055.994	13,055.146	0.848	14.353	86.966	13,142.112
$2v_1 + 3v_2^3 \leftarrow 0$	R(1, 1)	13,071.590	13,070.744	0.846	4.409	64.120	13,134.864
$3v_1 + 2v_2^2 \leftarrow 0$	^{t}R(1, 1)	13,332.884	13,332.307	0.577	1.324	64.120	13,396.427

Intensities are calculated at 600 K and normalized to the highest line in the range from 10,000–14,000 cm^{-1}

E(NU) result from **HYP** calculations. E(VR) = E(NU, HYP) + (E(VR, DVRJ) − E(NU, DVRJ)), i.e., the 'non-adiabatic' correction is calculated with the DVR-J code

The results of Kreckel et al. [14] were achieved at 55 K, but no intensities are published. The listed values are only useful for a comparison to the results of Morong et al. [13]

calculations for the rovibrational spectrum of H_3^+ we have reached this point. A promising approach for such a case is the theory of non-adiabatic PES [40–42]. These approaches have shown that in the case of H_3^+, the appropriate masses would be the "atomic mass" **NU23**$(\mathrm{NU23} = \mathrm{NU} + \frac{2}{3}m_e)$ for vibration and "nuclear mass" **NU** for rotation. Such a choice is meaningful if adiabatic corrections have been taken into account at the level of ab initio calculation and non-adiabatic contributions have to be simulated. Numerical calculations at low transition frequencies have already shown in the past quantitative differences (compared to 'best adapted' masses) of 0–2 cm^{-1} when using these different masses. Improvements are expected in the near future.

In the present work, the rovibrational eigenstates and the transitions were calculated in two different ways: (1) using

Table 3 Comparison between experimental (Morong et al. [13]) and theoretical transitions (in cm^{-1}) using nuclear mass NU

ν(EXP)	ν(NU)	$\Delta\nu_{EXP-NU}$	$\Delta\nu_{VR-NU}$	Γ	J	n	E′(NU)	Γ	J	n	E″(NU)
10,322.235	10,323.303	−1.068	−1.642	A_2'	3	0	516.908	A_2''	2	9	10,840.211
10,329.307	10,330.198	−0.891	−1.346	A_2'	6	0	995.915	A_2''	7	30	11,326.113
10,366.546	10,367.593	−1.047	−1.568	E′	2	0	169.309	E″	3	36	10,536.902
10,367.184	10,368.204	−1.020	−1.579	E″	2	0	237.369	E′	3	27	10,605.573
10,454.539	10,455.575	−1.036	−1.585	A_2''	3	0	315.365	A_2'	4	18	10,770.940
10,462.405	10,463.169	−0.764	−1.322	A_2'	6	0	995.915	A_2''	5	29	11,459.084
10,467.800	10,468.860	−1.060	−1.656	E″	2	0	237.369	E′	2	29	10,706.229
10,468.544	10,469.608	−1.064	−1.657	E″	3	0	494.792	E′	3	29	10,964.400
10,496.287	10,497.305	−1.018	−1.587	E″	5	0	729.044	E′	6	58	11,226.349
10,496.571	10,497.646	−1.075	−1.610	E″	2	0	237.369	E′	1	9	10,735.015
10,497.078	10,498.115	−1.037	−1.620	E′	4	0	502.059	E″	5	52	11,000.174
10,507.396	10,508.457	−1.061	−1.590	E′	3	0	428.042	E″	2	21	10,936.499
10,528.992	10,530.038	−1.046	−1.559	A_2''	4	0	658.748	A_2'	3	19	11,188.786
10,558.882	10,559.895	−1.013	−1.455	E″	5	0	729.044	E′	4	51	11,288.939
10,560.443	10,561.497	−1.054	−1.625	A_2'	3	0	516.908	A_2''	3	21	11,078.405
10,568.209	10,569.273	−1.064	−1.629	A_2'	1	0	86.966	A_2''	1	9	10,656.239
10,573.997	10,575.055	−1.058	−1.590	A_2''	4	0	658.748	A_2'	5	25	11,233.803
10,581.256	10,582.322	−1.066	−1.603	E″	1	0	64.128	E′	0	9	10,646.450
10,583.688	10,584.734	−1.046	−1.555	A_2''	3	0	315.365	A_2'	2	11	10,900.099
10,586.424	10,587.486	−1.062	−1.578	E′	2	0	169.309	E″	1	21	10,756.795
10,609.077	10,610.149	−1.072	−1.681	A_2''	3	0	315.365	A_2'	4	19	10,925.514
10,621.634	10,622.707	−1.073	−1.675	E′	2	0	169.309	E″	3	38	10,792.016
10,624.888	10,625.575	−0.687	−1.436	A_2''	4	0	658.748	A_2'	3	20	11,284.323
10,632.042	10,632.866	−0.824	−1.460	E′	4	0	502.059	E″	3	41	11,134.925
10,639.058	10,639.819	−0.761	−1.652	A_2'	5	0	1,271.325	A_2''	5	34	11,911.144
10,641.024	10,642.101	−1.077	−1.654	E″	1	0	64.128	E′	2	29	10,706.229
10,657.149	10,657.864	−0.715	−1.514	A_2'	3	0	516.908	A_2''	3	22	11,174.772
10,666.604	10,667.342	−0.738	−1.466	A_2''	5	0	1,080.536	A_2'	5	28	11,747.878
10,669.815	10,670.887	−1.072	−1.608	E″	1	0	64.128	E′	1	9	10,735.015
10,671.864	10,672.935	−1.071	−1.612	E″	2	0	237.369	E′	2	31	10,910.304
10,686.611	10,687.338	−0.727	−1.430	E′	4	0	502.059	E″	3	42	11,189.397
10,690.240	10,691.313	−1.073	−1.661	A_2''	4	0	658.748	A_2'	5	26	11,350.061
10,705.364	10,706.226	−0.862	−1.677	E′	3	0	428.042	E″	4	38	11,134.268
10,705.894	10,706.530	−0.636	−1.444	E′	3	0	428.042	E″	2	22	11,134.572
10,710.311	10,710.986	−0.675	−1.764	A_2''	4	0	658.748	A_2'	4	21	11,369.734
10,725.953	10,727.031	−1.078	−1.661	E″	2	0	237.369	E′	3	29	10,964.400
10,730.107	10,730.817	−0.710	−1.457	A_2''	3	0	315.365	A_2'	2	12	11,046.182
10,752.150	10,753.245	−1.095	−1.641	A_2'	1	0	86.966	A_2''	2	9	10,840.211
10,752.369	10,753.061	−0.692	−1.414	E′	2	0	169.309	E″	1	22	10,922.370
10,760.627	10,761.355	−0.728	−1.520	E′	3	0	428.042	E″	3	42	11,189.397
10,766.320	10,766.987	−0.667	−1.459	E″	2	0	237.369	E′	1	10	11,004.356
10,766.108	10,767.190	−1.082	−1.590	E′	2	0	169.309	E″	2	21	10,936.499
10,779.136	10,780.199	−1.063	−1.594	E′	3	0	428.042	E″	3	43	11,208.241
10,789.844	10,790.527	−0.683	−1.406	E″	2	0	237.369	E′	2	32	11,027.896
10,793.060	10,794.159	−1.099	−1.608	E′	4	1	768.511	E″	4	42	11,562.670
10,798.691	10,799.399	−0.708	−1.562	A_2'	3	0	516.908	A_2''	2	10	11,316.307
10,798.785	10,799.449	−0.664	−1.399	E″	1	0	64.128	E′	0	10	10,863.577
10,803.820	10,804.470	−0.650	−1.515	E″	3	0	494.792	E′	3	32	11,299.262
10,805.800	10,806.840	−1.040	−1.651	E″	3	0	494.792	E′	4	52	11,301.632
10,811.027	10,811.882	−0.855	−1.642	A_2''	5	0	1,080.536	A_2'	4	24	11,892.418

Table 3 continued

ν(EXP)	ν(NU)	$\Delta\nu_{EXP-NU}$	$\Delta\nu_{VR-NU}$	Γ	J	n	E′(NU)	Γ	J	n	E″(NU)
10,813.699	10,814.444	−0.745	−1.551	E″	3	0	494.792	E′	2	34	11,309.236
10,816.758	10,817.494	−0.736	−1.542	E″	4	0	833.621	E′	4	56	11,651.115
10,831.677	10,832.345	−0.668	−1.408	A_2'	1	0	86.966	A_2''	1	10	10,919.311
10,845.089	10,846.176	−1.087	−1.610	E″	1	0	64.128	E′	2	31	10,910.304
10,847.551	10,848.742	−1.191	−1.580	A_2''	4	0	658.748	A_2'	4	22	11,507.490
10,855.172	10,855.899	−0.727	−1.673	E′	4	1	768.511	E″	4	43	11,624.410
10,874.681	10,876.124	−1.443	−1.642	A_2'	6	0	995.915	A_2''	5	33	11,872.039
10,934.327	10,935.417	−1.090	−1.624	E″	2	0	237.369	E′	3	31	11,172.786
10,935.631	10,936.110	−0.479	−1.591	A_2'	3	0	516.908	A_2''	3	23	11,453.018
10,935.358	10,936.743	−1.385	−1.660	A_2'	3	0	516.908	A_2''	4	21	11,453.651
10,939.559	10,940.228	−0.669	−1.457	E″	1	0	64.128	E′	1	10	11,004.356
10,953.026	10,954.730	−1.704	−1.674	E″	5	0	729.044	E′	4	57	11,683.774
10,963.072	10,963.768	−0.696	−1.404	E″	1	0	64.128	E′	2	32	11,027.896
10,964.605	10,965.263	−0.658	−1.444	E′	2	0	169.309	E″	2	22	11,134.572
10,964.792	10,965.616	−0.824	−1.550	E′	2	0	169.309	E″	3	41	11,134.925
10,968.257	10,968.958	−0.701	−1.435	A_2''	3	0	315.365	A_2'	3	20	11,284.323
11,015.488	11,016.763	−1.275	−1.712	A_2''	4	0	658.748	A_2'	3	21	11,675.511
11,019.351	11,020.088	−0.737	−1.520	E′	2	0	169.309	E″	3	42	11,189.397
11,024.705	11,026.477	−1.772	−1.625	E″	3	0	494.792	E′	4	55	11,521.269
11,033.268	11,034.552	−1.284	−1.694	E′	4	0	502.059	E″	3	45	11,536.611
11,036.111	11,037.006	−0.895	−1.513	A_2'	6	0	995.915	A_2''	7	36	12,032.921
11,044.146	11,044.829	−0.683	−1.547	E″	1	0	64.128	E′	2	33	11,108.957
11,046.569	11,047.421	−0.852	−1.411	E″	5	0	729.044	E′	6	66	11,776.465
11,048.996	11,049.834	−0.838	−1.555	E′	4	0	502.059	E″	5	61	11,551.893
11,053.686	11,054.369	−0.683	−1.763	A_2''	3	0	315.365	A_2'	4	21	11,369.734
11,071.117	11,071.867	−0.750	−1.555	E″	2	0	237.369	E′	2	34	11,309.236
11,111.798	11,113.073	−1.275	−1.711	A_2''	3	0	315.365	A_2'	2	13	11,428.438
11,114.428	11,115.447	−1.019	−1.564	A_2''	4	0	658.748	A_2'	5	29	11,774.195
11,114.628	11,115.793	−1.165	−1.700	A_2'	5	0	1,271.325	A_2''	6	33	12,387.118
11,195.625	11,196.368	−0.743	−1.672	E′	3	0	428.042	E″	4	43	11,624.410
11,228.601	11,229.341	−0.740	−1.561	A_2'	1	0	86.966	A_2''	2	10	11,316.307
11,244.353	11,245.108	−0.755	−1.553	E″	1	0	64.128	E′	2	34	11,309.236
11,246.707	11,247.437	−0.730	−1.558	E″	2	0	237.369	E′	3	33	11,484.806
11,278.517	11,279.794	−1.277	−1.746	A_2'	3	0	516.908	A_2''	3	24	11,796.702
11,304.480	11,305.209	−0.729	−1.551	E′	2	0	169.309	E″	3	44	11,474.518
11,318.080	11,319.358	−1.278	−1.746	A_2'	1	0	86.966	A_2''	1	11	11,406.324
11,331.112	11,332.155	−1.043	−1.595	A_2'	6	0	995.915	A_2''	5	35	12,328.070
11,358.855	11,360.146	−1.291	−1.711	A_2''	3	0	315.365	A_2'	3	21	11,675.511
11,422.627	11,423.669	−1.042	−1.601	E″	5	0	729.044	E′	4	61	12,152.713
11,482.938	11,483.978	−1.040	−1.594	E′	4	0	502.059	E″	3	50	11,986.037
11,496.055	11,497.199	−1.044	−1.618	A2″	4	0	658.748	A_2'	3	23	12,155.947
11,494.835	11,495.983	−1.148	−1.642	A_2''	3	0	315.365	A_2'	2	14	11,811.348
11,496.796	11,497.672	−0.876	−1.661	E″	2	0	237.369	E′	3	34	11,735.041
11,503.614	11,504.900	−1.286	−1.751	A_2'	1	0	86.966	A_2''	2	11	11,591.866
11,515.921	11,516.746	−0.825	−1.607	E′	3	0	428.042	E″	4	45	11,944.788
11,556.914	11,557.715	−0.801	−1.638	A_2''	4	0	658.748	A_2'	5	31	12,216.463
11,562.798	11,563.842	−1.044	−1.706	A_2'	3	0	516.908	A_2''	3	26	12,080.750
11,564.098	11,565.193	−1.095	−1.742	E″	3	0	494.792	E′	3	38	12,059.985
11,571.876	11,572.925	−1.049	−1.625	A_2''	3	0	315.365	A_2'	2	15	11,888.290
11,576.154	11,577.053	−0.899	−1.640	A_2''	3	0	315.365	A_2'	4	24	11,892.418

Table 3 continued

v(EXP)	v(NU)	$\Delta v_{\mathrm{EXP-NU}}$	$\Delta v_{\mathrm{VR-NU}}$	Γ	J	n	E′(NU)	Γ	J	n	E″(NU)
11,578.494	11,579.533	−1.039	−1.607	E′	2	0	169.309	E″	1	26	11,748.842
11,606.157	11,607.239	−1.082	−1.664	A_2'	1	0	86.966	A_2''	1	12	11,694.205
11,618.521	11,619.599	−1.078	−1.769	A_2'	3	0	516.908	A_2''	4	23	12,136.507
11,668.916	11,669.435	−0.519	−1.813	A_2''	3	0	315.365	A_2'	4	25	11,984.800
11,691.577	11,692.663	−1.086	−1.757	A_2'	3	0	516.908	A_2''	3	27	12,209.571
11,694.789	11,695.929	−1.140	−1.774	E′	2	0	169.309	E″	3	49	11,865.238
11,707.268	11,708.382	−1.114	−1.716	E″	1	0	64.128	E′	2	38	11,772.510
11,707.801	11,708.852	−1.051	−1.653	E″	1	0	64.128	E′	1	12	11,772.980
11,728.382	11,729.398	−1.016	−1.740	E″	3	0	494.792	E′	4	63	12,224.190
11,788.272	11,789.326	−1.054	−1.644	E′	2	0	169.309	E″	2	26	11,958.635
11,793.656	11,794.712	−1.056	−1.735	E′	3	0	428.042	E″	4	48	12,222.754
11,835.025	11,836.017	−0.992	−1.744	A_2'	3	0	516.908	A_2''	4	25	12,352.925
11,839.565	11,840.582	−1.017	−1.617	A_2''	3	0	315.365	A_2'	3	23	12,155.947
11,854.459	11,855.577	−1.118	−1.727	A_2'	1	0	86.966	A_2''	2	12	11,942.543
11,892.128	11,895.482	−3.354	−1.901	E′	4	0	502.059	E″	5	73	12,397.541
11,947.074	11,948.523	−1.449	−1.354	A_2'	6	0	995.915	A_2''	5	41	12,944.438
11,953.935	11,955.121	−1.186	−1.831	A_2''	3	0	315.365	A_2'	4	27	12,270.486
11,978.640	11,979.734	−1.094	−1.790	A_2'	3	0	516.908	A_2''	4	26	12,496.642
12,097.708	12,098.841	−1.133	−1.761	E′	2	0	169.309	E″	3	53	12,268.150
12,102.469	12,102.644	−0.175	−1.673	A_2''	3	0	315.365	A_2'	4	28	12,418.009
12,116.353	12,118.002	−1.649	−1.738	A_2'	3	0	516.908	A_2''	3	30	12,634.910
12,181.941	12,183.029	−1.088	−1.716	A_2''	4	0	658.748	A_2'	3	27	12,841.777
12,207.905	12,209.223	−1.318	−1.639	E″	2	0	237.369	E′	2	44	12,446.592
12,222.032	12,223.407	−1.375	−1.607	E′	2	0	169.309	E″	1	30	12,392.716
12,246.368	12,247.449	−1.081	−1.807	A_2'	1	0	86.966	A_2''	2	13	12,334.415
12,246.574	12,247.495	−0.921	−1.759	A_2''	3	0	315.365	A_2'	2	17	12,562.860
12,253.670	12,254.999	−1.329	−1.651	A_2'	1	0	86.966	A_2''	1	14	12,341.965
12,314.977	12,315.967	−0.990	−1.722	A_2''	4	0	658.748	A_2'	4	32	12,974.715
12,320.975	12,322.101	−1.126	−1.733	A_2''	3	0	315.365	A_2'	4	29	12,637.466
12,331.180	12,332.250	−1.070	−1.864	A_2''	4	0	658.748	A_2'	5	37	12,990.998
12,419.140	12,420.636	−1.496	−1.667	A_2'	1	0	86.966	A_2''	1	15	12,507.602
12,502.614	12,503.835	−1.221	−1.734	A_2''	3	0	315.365	A_2'	2	19	12,819.200
12,525.302	12,526.412	−1.110	−1.715	A_2''	3	0	315.365	A_2'	3	27	12,841.777
12,536.621	12,537.860	−1.239	−1.879	A_2'	3	0	516.908	A_2''	4	29	13,054.768
12,623.171	12,624.247	−1.076	−1.698	E″	1	0	64.128	E′	1	15	12,688.375
12,658.335	12,659.350	−1.015	−1.721	A_2''	3	0	315.365	A_2'	4	32	12,974.715
12,897.888	12,899.129	−1.241	−1.889	A_2'	1	0	86.966	A_2''	2	15	12,986.095
13,056.013	13,056.990	−0.977	−1.844	A_2'	1	0	86.966	A_2''	2	16	13,143.956
13,597.367	13,598.561	−1.194	−1.821	A_2'	1	0	86.966	A_2''	1	19	13,685.527
13,606.093	13,607.112	−1.019	−1.965	A_2''	3	0	315.365	A_2'	4	39	13,922.477
13,676.446	13,679.581	−3.135	−1.873	A_2'	1	0	86.966	A_2''	1	20	13,766.547
10,827.764	10,828.470	−0.706	−1.505	A_2'	2	0	2,813.062	A_2'	3	31	13,641.532
11,265.189	11,262.746	2.443	−1.535	E″	2	2	3,410.261	E′	3	66	14,673.007

Initial (E′) and final (E″) rovibrational eigenstates (in cm^{-1}) with their symmetry assignment Γ, total angular momentum J and ordering index n are given E″(NU) and E′(NU) result from **HYP** calculations. E(VR) = E(NU, HYP) + (E(VR, DVRJ) − E(NU, DVRJ)), i.e. the 'nonadiabatic' correction is calculated with the DVR-J code

NU for rotation and vibration, and (2) using different effective masses for vibrational and rotational motion [10, 43] ($\mu_{\mathrm{V}} = 1.007642100$ amu, $\mu_{\mathrm{R}} = 1.0072764551$ amu). The latter variant is referred to as **VR** for vibrational and rotational mass. Polyansky and Tennyson (PT) [43] found that the kinetic energy expression had to be modified by an

Table 4 Comparison between experimental (Kreckel et al. [14]) and theoretical transitions (in cm^{-1}) using nuclear mass NU

v(EXP)	v(NU)	Δv_{EXP-NU}	Δv_{VR-NU}	Γ	J	n	E′(NU)	Γ	J	n	E″(NU)
11,228.598	11,229.341	−0.743	−1.561	A_2'	1	0	86.966	A_2''	2	10	11,316.307
11,244.350	11,245.108	−0.758	−1.553	E″	1	0	64.128	E′	2	34	11,309.236
11,258.975	11,260.254	−1.279	−1.736	E″	1	0	64.128	E′	0	11	11,324.382
11,342.587	11,343.879	−1.292	−1.737	E″	1	0	64.128	E′	1	11	11,408.007
11,465.505	11,466.797	−1.292	−1.751	E″	1	0	64.128	E′	2	35	11,530.925
11,511.373	11,512.670	−1.297	−1.742	E″	1	0	64.128	E′	2	36	11,576.798
11,594.276	11,595.351	−1.075	−1.625	E″	1	0	64.128	E′	0	12	11,659.479
11,707.257	11,708.382	−1.125	−1.716	E″	1	0	64.128	E′	2	38	11,772.510
11,707.797	11,708.852	−1.055	−1.653	E″	1	0	64.128	E′	1	12	11,772.980
11,882.376	11,883.470	−1.094	−1.688	E″	1	0	64.128	E′	2	39	11,947.598
12,018.812	12,020.014	−1.202	−1.783	A_2'	1	0	86.966	A_2''	1	13	12,106.980
12,086.738	12,087.964	−1.226	−1.843	E″	1	0	64.128	E′	2	41	12,152.092
12,239.242	12,240.559	−1.317	−1.640	E″	1	0	64.128	E′	0	14	12,304.687
12,373.325	12,374.560	−1.235	−1.845	E″	1	0	64.128	E′	1	14	12,438.688
12,381.135	12,382.464	−1.329	−1.637	E″	1	0	64.128	E′	2	44	12,446.592
12,413.257	12,414.829	−1.572	−1.624	E″	1	0	64.128	E′	0	15	12,478.957
12,419.127	12,420.636	−1.509	−1.667	A_2'	1	0	86.966	A_2''	1	15	12,507.602
12,623.160	12,624.247	−1.087	−1.698	E″	1	0	64.128	E′	1	15	12,688.375
12,678.683	12,679.758	−1.075	−1.780	E″	1	0	64.128	E′	2	48	12,743.886
12,897.877	12,899.129	−1.252	−1.889	A_2'	1	0	86.966	A_2''	2	15	12,986.095
13,055.994	13,056.990	−0.996	−1.844	A_2'	1	0	86.966	A_2''	2	16	13,143.956
13,071.590	13,072.551	−0.961	−1.807	E″	1	0	64.128	E′	2	52	13,136.679
13,332.884	13,334.316	−1.432	−2.009	E″	1	0	64.128	E′	2	53	13,398.444

Initial (E′) and final (E″) rovibrational eigenstates (in cm^{-1}) with their symmetry assignment Γ, total angular momentum J and ordering index n are given

E″(NU) and E′(NU) result from **HYP** calculations. E(VR) = E(NU, HYP) + (E(VR, DVRJ) − E(NU, DVRJ)), i.e. the 'non-adiabatic' correction is calculated with the DVR-J code

additional term if vibrational and rotational masses were not the same. This extra term is not large, but was found to be important especially for H_2D^+ making the residues compared to experimental values systematically smoother and smaller.

3 Results and discussion

Rovibrational eigenstates of H_3^+ and its various isotopologues have been analyzed in recent years by several groups [4, 8–10, 29, 43–52, 54]. Most of these calculations were based on less accurate PESs. The highly accurate CI-R12 (configuration interaction with an explicit linear r_{12} term in the wave function [8]) and GG PESs (including adiabatic and relativistic effects) used for H_3^+, H_2D^+, D_2H^+, and D_3^+ have improved the situation [2]; these potentials are termed RKJK [8] and CRJK [5]. In the most recent work of Schiffels et al. [29, 53] (using our GG PES [9]), band origins up to 13,000 cm^{-1} have been investigated, termed SAH(CRJK). They could show that non-adiabatic effects can be modeled by empirical corrections based on calculations using only the nuclear masses (termed SAHc), and that these empirical corrections had been proven very helpful for experimental groups to assign their new data [6, 7, 13, 14].

In the present paper, the rovibrational analysis is performed with the latest fitted potential, described in Ref. [4]. Three different numerical procedures for the calculation of the rovibrational energies and intensities have been used: (a) **DVR-J**: DVR with Jacobi coordinates [27] (using C_{2v}-symmetry; less accurate for energies above the barrier to linearity, i.e., this might result from a singularity in the kinetic energy operator for linear geometries; for further discussion see Ref. [4]), (b) **HYP**: hyperspherical coordinates with hyperspherical harmonics [28] (keeping D_{3h}-symmetry; no numerical problems for energies higher than the barrier to linearity), and (c) **FD-J**: filter-diagonalization with Jacobi coordinates (C_{2v}-symmetry; used for cross check of the DVR-J code; results are in close agreement with **HYP** calculations).

New results of transitions above the barrier to linearity in the frequency range of 10,000–14,000 cm^{-1} will be presented. The results (see Tables 1, 2, 3, 4) are compared to the most recent experimental results of Gottfried [6, 7], Morong et al. [13], and Kreckel et al. [14]. Whereas for most of the experimental transitions, the uncertainty is claimed to be in the range of ≈ 0.01 cm^{-1}, nothing is specified for the quality of experimental relative intensities. The calculated rovibrational energies are based on **HYP** calculations (using the **NU** masses), and the data were selected with respect to intensity calculations (using DVR-J) in the given frequency range with relative intensities mostly larger than 1%. In addition, a list of transitions (with relative intensities >5%) not seen experimentally, are given in Table 6. The energy corrections E(VR) − E(NU) (in the range of 0–2 cm^{-1}), which take into account the influence of non-adiabaticity using **VR** masses are calculated with the **DVR-J** code, because the necessary change of the kinetic energy hamiltonian is implemented only within DVR-J and the calculated eigenstates are in most cases not too different from the numerically correct ones, i.e., **HYP** calculations. In summary, E(NU) are **HYP** calculations and E(VR) = E(NU, HYP) + (E(VR, DVRJ) − E(NU, DVRJ)). So, the frequencies are 'mainly' based on **HYP** calculations. Since the **HYP** calculations provide the correct symmetry for the eigenfunctions, the selection of symmetry allowed transitions is based only on these calculations, whereas the Einstein coefficients for intensities are calculated with the **DVR-J** code. Less converged **DVR-J** calculations can lead to suboptimal intensity values, and therefore mismatches compared to experimental intensities might be related to that.

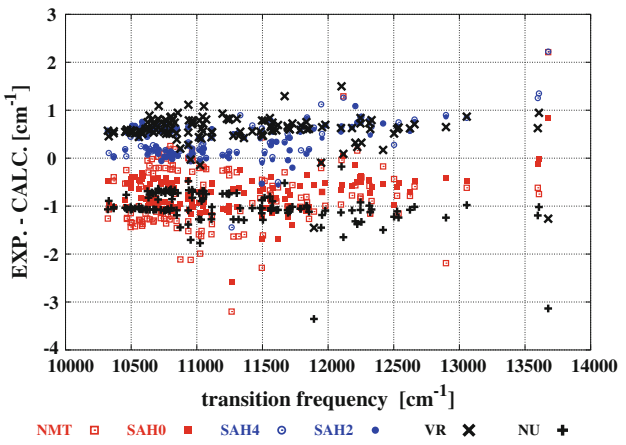

Fig. 1 The differences between the experimentally observed (Morong et al. [13]) and theoretically predicted frequencies (in cm^{-1}). In addition to the results obtained within the current study (VR and NU masses), the literature data are also shown: NMT [46], SAH0 [53], SAH4 and SAH2. All data, except those of the present study (VR, NU), are taken from Table 3 in Ref. [13]

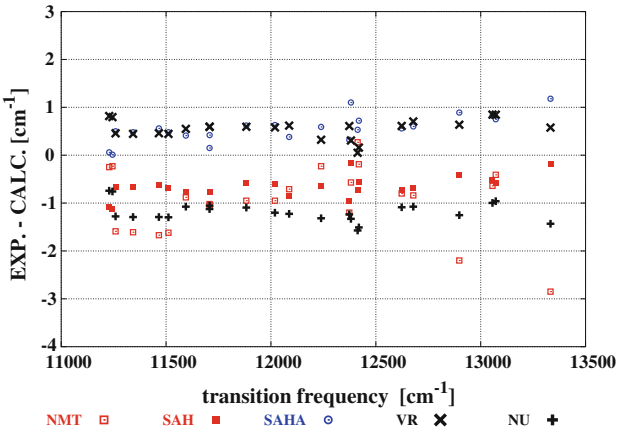

Fig. 2 The differences between the experimentally observed (Kreckel et al. [14]) and theoretically predicted frequencies (in cm^{-1}). In addition to the results obtained within the current study (VR, NU), the literature data are also shown: NMT [46], unadjusted SAH [53] and adjusted SAHA [14]. All data, except present study, are taken from Table 2 in Ref. [14]

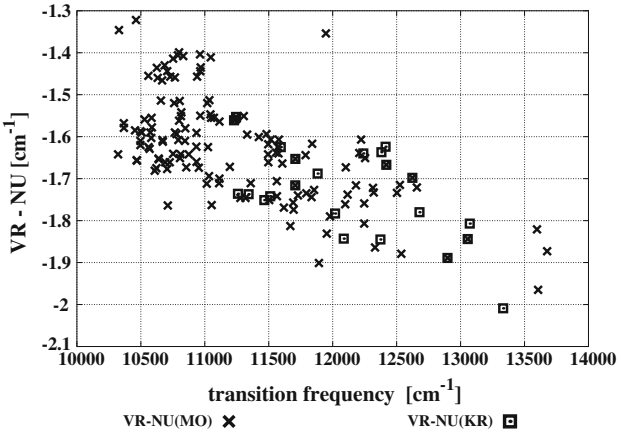

Fig. 3 The differences between theoretically predicted frequencies (in cm^{-1}) using VR and NU masses for those frequencies measured by Morong et al. (MO) [13] and Kreckel et al. (KR) [14]

For the calculation of the spectrum we assumed a temperature of $T = 600$ K (as claimed in the work of Morong et al. [13]; $T = 300$ K calculations show larger deviations compared to experiment). The intensities of the transitions, computed with the **DVR-J** suite, are based on the dipole moment functions calculated on CI-R12 level [8]. In the present study, we have used the assignment, especially of the final state, already given in the literature [13, 14], because in several cases we could not clearly assign the transitions to particular vibrational quantum numbers of the final state. The effect of non-adiabaticity, i.e., a comparison of **VR** and **NU** results, is plotted in Figs. 1, 2, and 3. With **NU** masses the theoretical frequencies are slightly too large $\Delta\nu_{\text{exp-calc}} \in \langle -0.5, -1.5 \rangle$ cm^{-1}, whereas the correction with **VR** is roughly 1 cm^{-1} towards lower frequencies. The

Table 5 Comparison among observed (Morong et al. [13] and Kreckel et al. [14]) and theoretical frequencies (obs. calc.) (in cm^{-1})

	NMT (DPT)	SAH (CRJK)	SAH4	SAH2	**NU**	**VR**
A: Comparison with Ref. [13]						
Average error	−0.756	−0.736	0.406	0.353	−1.026	0.603
rms	0.997	0.807	0.544	0.466	1.087	0.683
Std. deviation (calc.)	0.635	0.332	0.363	0.306	0.360	0.322
B: Comparison with Ref. [14]						
Average error	−0.756	−0.679	0.555		−1.183	0.549
rms	1.194	0.719	0.621		1.200	0.584
Std. deviation (calc.)	0.716	0.240	0.286		0.206	0.203

The theoretically predicted transitions are from the calculations by NMT [46], SAH, SAH4, SAH2, SAHad [53] (as given in Table 3 of Ref. [13] and Table 2 of Ref. [14]), and present results (**VR** and **NU**). The labels in parenthesis refer to the potential energy surfaces used: RKJK [8], DPT [56], CRJK [5]. All new results (**NU, VR**) are based on our new BCJK potential [4]. Part A, Errors are calculated from the first 141 transitions in Table 1 and 3 (EXP, Morong et al. [13]) with initial vibrational ground state; Part B, all data from Tables 2 and 4 (EXP, Kreckel et al. [14]) are taken (23 transitions)

choice of the **VR** masses requires improvement based on rigorous theory considerations (see e.g., [42]). Some frequencies do not fit into this set of data. The intensity of the transitions deviates stronger from the experimental ones for the frequency range of 10,000–14,000 cm^{-1} than for lower frequency ranges. The reason for this deviation is not yet clear, but might be related to some poorly converged DVR-J calculations (used for intensities) for energies above the barrier to linearity.

In Table 5 and Figs. 1, 2, we compare our results with earlier calculations [46, 49, 53]. These were mostly based on a potential in which the fit was not sufficiently supported by ab initio data in the energy region above the barrier to linearity (see the discussion of RMS values in Sect. 2.1). Comparisons with calculations based on lower quality ab initio data have been neglected. The best-suited comparison with other theoretical investigations is the one with SAH(CRJK) [29, 53] (see Table 5 and Figs. 1, 2).

In SAH the same program (**HYP**), **NU** mass and fit (CRJK: [5, 9]) were used.

The differences between our new and SAH results refer mainly to the changes in the representation of the BCJK- [4] versus CRJK- [5] potential. This leads to an increase or decrease in the transition frequencies compared to experiment, because non-adiabatic effects have not been included rigorously. As a result, our **NU** calculations (Table 5) show a slight increase in the average error and RMS value (individual comparisons with the data of Ref. [13] and [14] are termed MO and KR) (MO −1.026, 1.087; KR −1.183, 1.200 cm^{-1}) compared to SAH (MO −0.736, 0.807; KR −0.679, 0.719 cm^{-1}), whereas the standard deviation (MO 0.360; KR 0.206 cm^{-1}) is very similar to the average error in SAH (MO 0.332; KR 0.240 cm^{-1}). For the **VR** calculations, the standard deviation is further reduced (MO 0.603;

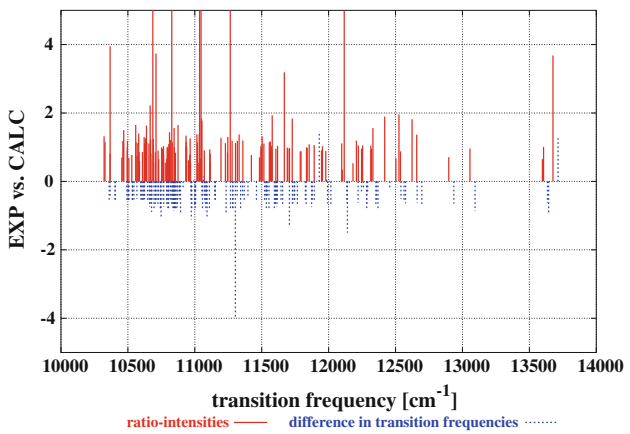

Fig. 4 Experiment (Morong et al. [13]) versus calculation: ratio of the relative intensities (*top*) and difference in the transition frequencies (in cm^{-1}) (*bottom*) using VR masses

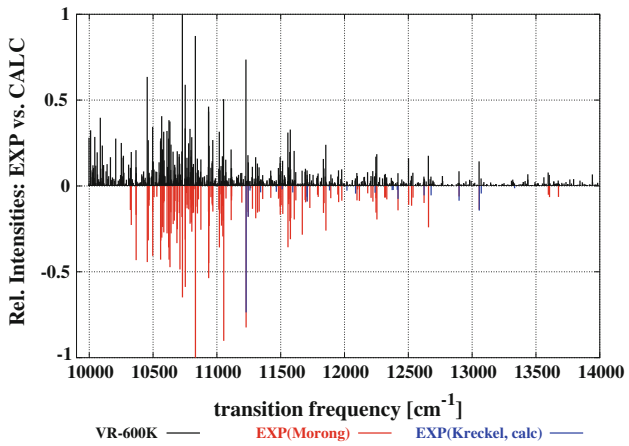

Fig. 5 Proposed spectrum (*top*) of H_3^+ for 600 K in the range 10,000–14,000 cm^{-1} (more than 10,000 transitions) in comparison with experiment (*bottom*: MO + KR; ca. 160 transitions). *Bottom* part for the experimental transitions of KR (Kreckel et al. [14]), the proposed calculated values are shown

Table 6 Proposal of the strongest transitions with relative intensities >5% ($T = 600$ K) in the region of 10,000–14,000 cm^{-1}, yet not measured experimentally

ν(VR)	Intens. (%)	$\Delta\nu_{VR-NU}$	Γ	J	n	E′(NU)	Γ	J	n	E″(NU)
9,999.432	28.1	−1.431	E′	4	0	502.059	E″	5	46	10,501.491
10,011.685	32.4	−1.476	E′	3	0	428.042	E″	4	31	10,439.727
10,023.920	5.1	−1.454	E″	3	0	494.792	E′	4	42	10,518.712
10,025.915	8.0	−1.558	E″	1	0	64.128	E′	1	8	10,090.043
10,029.980	12.1	−1.562	E″	2	0	237.369	E′	2	26	10,267.349
10,032.049	9.7	−1.580	E″	3	0	494.792	E′	3	26	10,526.841
10,033.713	5.4	−1.566	E″	4	0	833.621	E′	4	46	10,867.334
10,013.417	9.1	−1.428	E″	7	0	1,302.191	E′	8	62	11,315.608
10,035.775	10.5	−1.585	A_2'	3	0	516.908	A_2''	3	18	10,552.683
10,044.938	28.6	−1.566	A_2'	1	0	86.966	A_2''	1	8	10,131.904
10,052.508	11.9	−1.581	A_2'	3	0	516.908	A_2''	3	19	10,569.416
10,063.765	19.6	−1.498	E″	3	0	494.792	E′	4	43	10,558.557
10,065.969	6.7	−1.428	E″	5	0	729.044	E′	6	52	10,795.013
10,088.171	39.7	−1.500	A_2'	3	0	516.908	A_2''	4	17	10,605.079
10,091.114	10.1	−1.617	A_2''	5	0	1,080.536	A_2'	6	25	11,171.650
10,103.578	23.5	−1.477	A_2''	4	0	658.748	A_2'	5	22	10,762.326
10,113.531	12.2	−1.543	E′	4	1	768.511	E″	5	50	10,882.042
10,140.730	12.7	−1.483	E′	5	0	929.014	E″	6	46	11,069.744
10,133.026	8.5	−1.436	A_2'	7	0	1,586.657	A_2''	8	27	11,719.683
10,153.267	5.7	−1.591	A_2''	5	0	1,080.536	A_2'	5	25	11,233.803
10,167.163	16.8	−1.464	E″	4	0	833.621	E′	5	43	11,000.784
10,208.302	27.6	−1.438	A_2''	4	0	658.748	A_2'	5	23	10,867.050
10,246.564	6.4	−1.614	E′	4	1	768.511	E″	5	53	11,015.075
10,252.417	25.0	−1.578	A_2'	1	0	86.966	A_2''	2	8	10,339.383
10,256.712	16.5	−1.577	E″	1	0	64.128	E′	2	27	10,320.840
10,260.364	5.6	−1.541	E′	5	1	1,187.160	E″	6	51	11,447.524
10,269.091	17.6	−1.576	A_2''	5	0	1,080.536	A_2'	6	27	11,349.627
10,272.957	7.7	−1.585	E″	5	1	1,250.366	E′	6	62	11,523.323
10,309.600	12.4	−1.566	A_2'	5	0	1,271.325	A_2''	6	26	11,580.925
10,370.233	7.5	−1.618	E″	7	0	1,302.191	E′	8	66	11,672.424
10,415.512	5.5	−1.608	E″	3	0	494.792	E′	2	31	10,910.304
10,412.819	6.8	−1.342	E″	7	0	1,302.191	E′	6	65	11,715.010
10,425.074	5.9	−1.568	A_2''	4	0	658.748	A_2'	3	18	11,083.822
10,426.954	8.5	−1.581	A_2''	5	0	1,080.536	A_2'	4	22	11,507.490
10,493.045	9.3	−1.591	E′	3	0	428.042	E″	4	36	10,921.087
10,488.772	5.6	−1.441	A_2'	7	0	1,586.657	A_2''	6	29	12,075.429
10,502.711	14.0	−1.599	A_2'	3	0	516.908	A_2''	4	19	11,019.619
10,523.766	8.4	−1.460	A_2'	6	0	995.915	A_2''	7	32	11,519.681
10,548.769	13.8	−1.476	A_2'	6	0	995.915	A_2''	5	30	11,544.684
10,556.338	7.9	−1.535	E′	4	0	502.059	E″	3	39	11,058.397
10,554.951	6.4	−1.613	A_2''	5	0	1,080.536	A_2'	6	29	11,635.487
10,562.933	6.7	−1.377	E′	5	0	929.014	E″	4	41	11,491.947
10,590.934	6.0	−1.592	E″	6	0	1,238.504	E′	7	58	11,829.438
10,596.033	5.7	−1.544	A_2'	7	0	1,586.657	A_2''	8	32	12,182.690
10,614.886	11.1	−1.657	E′	5	0	929.014	E″	6	52	11,543.900
10,636.501	6.5	−1.420	E″	5	0	729.044	E′	4	54	11,365.545
10,677.994	6.7	−1.620	E″	3	0	494.792	E′	3	31	11,172.786

Table 6 continued

ν(VR)	Intens. (%)	$\Delta\nu_{VR-NU}$	Γ	J	n	E′(NU)	Γ	J	n	E″(NU)
10,695.396	6.3	−1.584	E′	5	0	929.014	E″	4	43	11,624.410
10,706.007	7.1	−1.552	E′	4	1	768.511	E″	3	44	11,474.518
10,768.457	5.4	−1.567	A_2''	3	0	315.365	A_2'	3	18	11,083.822
10,716.388	6.7	−1.723	A_2''	5	0	1,080.536	A_2'	6	31	11,796.924
10,783.382	5.1	−1.646	E′	4	1	768.511	E″	5	61	11,551.893
10,803.244	5.3	−1.585	E″	7	0	1,302.191	E′	6	72	12,105.435
10,857.827	5.8	−1.439	E′	2	0	169.309	E″	1	23	11,027.136
10,873.421	8.3	−1.558	A_2''	3	0	315.365	A_2'	3	19	11,188.786
10,888.426	5.0	−1.655	E″	4	0	833.621	E′	5	51	11,722.047
10,901.420	5.2	−1.666	E″	4	0	833.621	E′	3	34	11,735.041
10,904.431	5.7	−1.531	E′	3	0	428.042	E″	2	23	11,332.473
10,923.914	6.5	−1.600	A_2''	5	0	1,080.536	A_2'	5	30	12,004.450
11,063.905	6.1	−1.465	E′	3	0	428.042	E″	4	41	11,491.947
11,071.042	15.3	−1.829	E′	4	0	502.059	E″	5	62	11,573.101
11,118.072	5.4	−1.670	E″	4	0	833.621	E′	5	55	11,951.693
11,156.139	5.5	−1.665	A_2'	3	0	516.908	A_2''	4	22	11,673.047
11,171.180	6.5	−1.494	E″	5	0	729.044	E′	6	69	11,900.224
11,188.594	7.5	−1.724	E′	2	0	169.309	E″	1	24	11,357.903
11,223.422	5.8	−1.759	A_2''	4	0	658.748	A_2'	4	23	11,882.170
11,276.046	5.1	−1.754	E″	3	0	494.792	E′	3	35	11,770.838
11,326.052	5.9	−1.814	A_2''	4	0	658.748	A_2'	4	25	11,984.800
11,425.635	6.0	−1.728	A_2'	3	0	516.908	A_2''	2	12	11,942.543
11,530.593	6.2	−1.644	E′	3	0	428.042	E″	2	26	11,958.635
11,535.141	5.2	−1.718	E″	2	0	237.369	E′	2	38	11,772.510
11,572.590	6.3	−1.710	E′	4	0	502.059	E″	5	67	12,074.649
11,755.865	6.5	−1.810	E′	4	1	768.511	E″	5	76	12,524.376
11,850.824	5.5	−1.924	E″	5	0	729.044	E′	6	83	12,579.868
12,158.798	5.3	−1.806	A_2'	3	0	516.908	A_2''	4	27	12,675.706
12,153.513	5.1	−1.704	E′	4	0	502.059	E″	3	59	12,655.572
12,222.201	5.2	−1.878	E″	2	0	237.369	E′	3	41	12,459.570
12,237.768	5.6	−1.820	E′	3	0	428.042	E″	4	53	12,665.810
12,277.341	5.0	−1.818	A_2''	5	0	1,080.536	A_2'	6	45	13,357.877
12,769.341	5.8	−1.868	A_2'	3	0	516.908	A_2''	3	35	13,286.249
13,438.541	6.8	−1.852	A_2''	3	0	315.365	A_2'	2	23	13,753.906
13,564.565	5.1	−1.702	E″	2	0	237.369	E′	2	59	13,801.934
13,944.518	6.7	−1.932	A_2'	1	0	86.966	A_2''	2	19	14,031.484

KR 0.549 cm^{-1}). In the former work [4] we have used, in addition, the empirical shifts provided by Schiffels et al. [29], which improved the comparison to the experimental data. The investigation of these empirical shifts provides some hint which are the main contributions to the non-adiabatic corrections. Another way to estimate the non-adiabatic contributions is proposed by Alijah and Hinze [55] in calculating rovibrational expectation values of the linear term in a Taylor expansion of the potential energy surface with respect to each individual rovibrational motion. These contributions can be fitted to known experimental transition frequencies, so that the fit can be used for the estimation of corrections of only theoretically known transitions. This had been tested so far for H_2. Our aim is to put more effort in calculating the non-adiabatic corrections based on a rigorous theory to represent the rovibrational spectrum of a given energy region with sub-wavenumber accuracy [40, 42].

As one can see from Table 1, the difference in the transition frequencies ν (exp. calc.) is positive for all states except three (average error of about 0.603). Negative deviations by more than 1 cm^{-1} are not explainable: in

some cases the intensities differ by far more than the average (see also Fig. 4).

In Fig. 3, we see a steady increase of deviation between the VR- and NU-mass results, i.e., rovibrational energies experience a larger portion of the potential energy surface where the energy difference between the electronically ground and excited state is experienced.

In Fig. 4, we present the ratio of experimental and calculated (exp. calc.) relative intensities, together with deviations in transition frequencies using the VR-mass in the calculation. For 11 out of 143 transitions, the deviations for the ratio in intensities are larger by a factor of 2 (most of them are in the range of 0.8–1.2; the two intensities (exp. calc.) are given in Table 1). It is not clear why there is such a mismatch in 11 cases, except that the different experimental setups have been used or some intensity calculations are poorly converged. In one case (last line in Table 1), the mismatch is by four orders of magnitude and the transition deviates by ≈ 4 cm^{-1}. Probably the transition is not related to H_3^+.

In Fig. 5, we propose the spectrum for 600 K in the range of 10,000–14,000 cm^{-1}. Compared to the known experimental transitions (143 from Ref. [13] and 23 from Ref. [14]) more than 10,000 transitions with relative intensities between 1 and 10^{-6} are plotted. The most strongest intensities in the given energy range of 10,000–14,000 cm^{-1} that have been not experimentally detected are given in Table 6. These include P, Q, and R transitions; in case of higher rotational states ($J > 5$), the magnitude of the intensity might be not very reliable. As one can see from Table 2, the detection technique used by Kreckel et al. [14] is able to find transitions at relatively weak intensities. The stronger transitions in the accessible range were already observed by Gottfried et al. [6, 13]. But in both experiments (MO and KR), weak transitions below a relative intensity (with respect to the strongest intensity in the range of 10,000–14,000 cm^{-1}) of $\approx 2\%$ have not been measured up to now. There is also experimentally a gap of missing transition between 8,200 and 10,300 cm^{-1}.

4 Summary

In this paper, we report on new results of ab initio calculations of selected rovibrational transitions of H_3^+ in the range of 10,000–14,000 cm^{-1} and compare them with experimental data available in the literature. The deviation of the computed rovibronic frequencies of <1.5cm^{-1} is related to non-adiabatic effects. By choosing two different masses for rotational and vibrational motion, non-adiabatic effects have been simulated in an empirical way. As a final result, the deviations became only slightly smaller and have changed the sign. This is a strong indication that one needs an effective, coordinate-depending mass rather than constant mass as already discussed in Ref. [40, 42]. Based on the improvements gained for the non-adiabatic contributions to the rovibrational energies of H_2 and H_2^+ and its isotopologes we hope that similar work can be done for triatomics like H_3^+. Work is now in progress to include mass effects for the different individual rovibrational energies based on a more rigorous theory.

Acknowledgments Support from HRZ-Siegen (Rubens-Cluster) is gratefully acknowledged. Thanks to A. Alijah and M. Khoma for many stimulating discussions. This work is supported by the Deutsche Forschungsgemeinschaft.

References

1. Oka T (2006) Phil Trans R Soc A 364:2847
2. Kutzelnigg W, Jaquet R (2006) Phil Trans R Soc A 364:2855
3. Alijah A, Varandas AJC (2006) Phil Trans R Soc A 364:2889
4. Bachorz RA, Cencek W, Jaquet R, Komasa J (2009) J Chem Phys 131:024105
5. Cencek W, Rychlewski J, Jaquet R, Kutzelnigg W (1998) J Chem Phys 108:2831
6. Gottfried JL, McCall BJ, Oka T (2003) J Chem Phys 119:10890
7. Gottfried J (2006) Phil Trans R Soc A 364:2917
8. Röhse R, Kutzelnigg W, Jaquet R, Klopper W (1994) J Chem Phys 101:2231
9. Jaquet R, Cencek W, Kutzelnigg W, Rychlewski J (1998) J Chem Phys 108:2837
10. Jaquet R (1999) Chem Phys Lett 302:27
11. Jaquet R (2003) In: Rychlewski J (ed) Explicitly correlated wave functions in chemistry and physics. Kluwer Academic Publisher, Dordrecht, pp 503–544
12. Rychlewski J, Komasa J (2003) In: Rychlewski J (ed) Explicitly correlated wave functions in chemistry and physics. Kluwer Academic Publisher, Dordrecht, p 91
13. Morong CP, Gottfried JL, Oka T (2009) J Mol Struct 255:13
14. Kreckel H, Bing D, Reinhardt S, Petrignani A (2008) M Berg A Wolf J Chem Phys 129:164312
15. Schlemmer S, Kuhn T, Lescop E, Gerlich D (1999) Int J Mass Spectrom 185:589
16. Handy NC, Yamaguchi Y, Schaefer HF III (1986) J Chem Phys 84:4481
17. Kutzelnigg W (1997) Mol Phys 90:909
18. Bardo RD, Wolfsberg M (1978) J Chem Phys 68:2686
19. Kutzelnigg W (1989) Z Phys D 11:15
20. Kutzelnigg W (1990) Z Phys D 15:27
21. Rutkowski A (1986) J Phys B 19:149
22. Rutkowski A (1986) J Phys B 19:3431
23. Rutkowski A (1986) J Phys B 19:3443
24. Cencek W, Kutzelnigg W (1996) J Chem Phys 105:5878
25. Ottschofski E, Kutzelnigg W (1997) J Chem Phys 106:6634
26. Tennyson J (2000) In: Jensen P, Bunker PR (eds) Computational molecular spectroscopy. Wiley, p 305
27. Tennyson J, Henderson JR, Fulton NG (1995) Comput Phys Commun 86:175
28. Wolniewicz L, Hinze J (1994) J Chem Phys 101:9817
29. Schiffels P, Alijah A, Hinze J (2003) Mol Phys 101:175
30. Mandelshtam VA, Taylor HS (1995). J Chem Phys 102:7390
31. Morari C, Jaquet R (2005) J Phys Chem A 109:3396
32. Weiss J (2000) PhD-thesis, Göttingen

33. Weiss J, Schinke R, Mandelshtam VA (2000) J Chem Phys 113:4588
34. Watson JKG (1984). J Mol Struct 103:350
35. Lindsay CM, McCall BJ (2001) J Mol Struct 210:60
36. Moss RE (1996) Mol Phys 89:195
37. Bunker PR, Moss RE (1977) Mol Phys 33:417
38. Kutzelnigg W (1997) Mol Phys 90:909
39. Herman RM, Asgharian A (1966) J Mol Struct 19:305
40. Jaquet R, Kutzelnigg W (2008) Chem Phys 346:69
41. Pachucki K, Komasa J (2008) J Chem Phys 129:034102
42. Pachucki K, Komasa J (2009) J Chem Phys 130:164314
43. Polyansky OL Tennyson J (1999) J Chem Phys 110:5056
44. Jaquet R, Röhse R (1995) Mol Phys 84:291
45. Jaquet R (2002) Spectrochim Acta Part A 58:691
46. Neale L, Miller S, Tennyson J (1996) Astrophys J Lett 464:516
47. Dinelli BM, Le Sueur CR, Tennyson J, Amos RD (1995) Chem Phys Lett 232:295
48. Kostin MA, Polyansky OL, Tennyson J (2002) J Chem Phys 116:7564
49. Alijah A, Hinze J, Wolniewicz L (1995) Mol Phys 85:1105
50. Alijah A, Wolniewicz L, Hinze J (1995) Mol Phys 85:1125
51. Alijah A, Beuger M (1996) Mol Phys 88:497
52. Hinze J, Alijah A, Wolniewicz L (1998) Polish J Chem 72:1293
53. Schiffels P, Alijah A, Hinze J (2003) Mol Phys 101:189
54. Velilla L, Lepetit B, Aguado A, Beswick JA, Paniagua M (2008) J Chem Phys 129:084307
55. Alijah A, Hinze J (2006) Phil Trans R Soc A 364:2877
56. Dinelli BM, Polyansky OL, Tennyson J (1995) J Chem Phys 103:10433